PHOTONICS Research

Direct demonstration of carrier distribution and recombination within step-bunched UV-LEDs

Houqiang Xu,[1,2] Jiean Jiang,[1,2,3] Li Chen,[1] Jason Hoo,[4] Long Yan,[4] Shiping Guo,[4] Cai Shen,[1] Yanping Wei,[1] Hua Shao,[5] Zi-Hui Zhang,[5] Wei Guo,[1,2,6] and Jichun Ye[1,2,7]

[1]Ningbo Institute of Materials Technology and Engineering, Chinese Academy of Sciences, Ningbo 315201, China
[2]University of Chinese Academy of Sciences, Beijing 100049, China
[3]School of Physical Science and Technology, ShanghaiTech University, Shanghai 201210, China
[4]Advanced Micro-Fabrication Equipment Inc., Shanghai 201201, China
[5]Institute of Micro-Nano Photoelectron and Electromagnetic Technology Innovation, School of Electronics and Information Engineering, Hebei University of Technology, Tianjin 300401, China
[6]e-mail: guowei@nimte.ac.cn
[7]e-mail: jichun.ye@nimte.ac.cn

Received 6 October 2020; revised 9 January 2021; accepted 16 February 2021; posted 2 March 2021 (Doc. ID 411832); published 26 April 2021

AlGaN-based solid state UV emitters have many advantages over conventional UV sources. However, UV-LEDs still suffer from numerous challenges, including low quantum efficiency compared to their blue LED counterparts. One of the inherent reasons is a lack of carrier localization effect inside fully miscible AlGaN alloys. In the pursuit of phase separation and carrier localization inside the active region of AlGaN UV-LED, utilization of highly misoriented substrates proves to be useful, yet the carrier distribution and recombination mechanism in such structures has seldom been reported. In this paper, a UV-LED with step-bunched surface morphology was designed and fabricated, and the internal mechanism of high internal quantum efficiency was studied in detail. The correlation between microscale current distribution and surface morphology was provided, directly demonstrating that current prefers to flow through the step edges of the epitaxial layers. Experimental results were further supported by numerical simulation. It was found that efficient radiative recombination centers were formed in the inclined quantum well regions. A schematic three-dimensional energy band structure of the multiple quantum wells (MQWs) across the step was proposed and helps in further understanding the luminescence behavior of LEDs grown on misoriented substrates. Finally, a general principle to achieve carrier localization was proposed, which is valid for most ternary III-V semiconductors exhibiting phase separation.

https://doi.org/10.1364/PRJ.411832

1. INTRODUCTION

AlGaN-based ultraviolet light-emitting diodes (UV LEDs), with the advantages of compact structure, long lifetime, and controllable wavelength, are promising in numerous applications, such as air/water sterilization [1], surface disinfection [2], plant growth [3], and the detection of biochemical agents [1,4,5]. However, the development of AlGaN-based UV LEDs is still in its infancy compared to InGaN-based blue and green LEDs, owing to various scientific and technical challenges, such as inferior crystal quality [6], low doping efficiency of high Al composition p-type layers [7], poor light extraction efficiency due to dominant TM light polarization [8], and UV light absorption by p-GaN and metal contacts [9]. As a matter of fact, the widely reported external quantum efficiencies (EQEs) of AlGaN-based UV LEDs are mostly below 5% [10–13].

Internal quantum efficiency (IQE) is one of the most important factors contributing to the EQE of UV LEDs. Ban *et al.* have demonstrated that in order to increase IQE to a decent value such as 50%, threading dislocation density (TDD) needs to remain as low as 3×10^8 cm^{-2} [14]. This poses a stringent requirement on AlN or AlGaN epitaxial growth, as the mobility of Al atoms is inherently low compared to Ga. Recently, researchers have demonstrated the defect-insensitive behaviors of the UV multiple quantum wells (MQWs) and UV LEDs with high IQE values and strong luminescence intensities. This was achieved by epitaxial growth of high-Al content AlGaN and heterostructures on a sapphire substrate with a high misorientation angle. In our previous study, IQE as high as 90% was obtained from the MQWs grown on a 4° misoriented sapphire substrate, even if the TDD was in the range of 10^9 cm^{-2} [15,16]. It has been verified that composition

fluctuation occurred along the step-bunching region of the epitaxial thin film. Higher Ga content is induced near the step edges during growth due to relatively higher surface diffusivity of Ga atoms [17–19]. This leads to enhanced carrier confinement within the potential minimum of the active region and greatly improved IQE [20].

Despite progress made in the fabrication of UV LEDs on misoriented substrates, the physics of carrier transportation and recombination in the active regions is still poorly understood. In our previous work, it was reported that radiative recombination center formed in the step edge area with the support of μ-cathodoluminescence (CL) characterization [15]. Kojima *et al*. further proposed a carrier localization model, together with a hypothesis of current paths in the uneven quantum wells (QWs) [18,21]. But this model is based upon optical pumping results such as photoluminescence (PL) characterization. Direct evidence on the carrier localization effect during electrical injection is still lacking. Under optical pumping, photogenerated carriers are uniformly produced in the exposed area. Nevertheless, under electrical injection, the transportation and recombination of carriers are dominated by the built-in electric field and heterojunction barrier. To make things even more complex, current will selectively flow through a potential minimum in a 3D configuration under external bias, yet the physics of vertical and lateral transport through MQW structures is still poorly understood [15]. In other words, whether the existence of inclined quantum wells (IQWs) will enhance or suppress the carrier localization effect under electrical injection needs to be further investigated, which is critically important during future design and fabrication of UV LEDs. Furthermore, since no information was given with regard to the relationship between threading dislocations and Ga-rich regions near the step-bunched regions, one would intuitively argue that step bunching would deteriorate the crystalline quality of AlGaN and lead to current leakage paths. This concern has yet to be elucidated.

In this work, the dependence of current distribution on the surface morphology in the sub-300 nm emission of UV-LEDs grown on misoriented sapphire substrate was investigated in detail. It is demonstrated that as forward bias increases, the current flows through the step edge first, and then expands to adjacent regions. The macro-step structure was also modeled and simulated according to transmission electron microscopy observations. Current paths are formed in the step edges owing to Ga enrichment. Further investigations found that the IQWs have better carrier confinement due to both smaller bandgap and spontaneous polarization compared to adjacent flat QWs. This comprehensive study clearly illustrates that a UV LED grown on misoriented substrate is only one of the many techniques to achieve phase separation and carrier localization, which provides a new perspective in the realization of high-efficiency UV emitters.

2. EXPERIMENT SECTION

AlGaN-based UV LEDs were grown on 2-inch *c*-plane sapphire substrates with an approximate 1° misorientation angle toward the *m* plane using an AMEC Prismo HiT_3 MOCVD reactor in H_2 ambient. Trimethylaluminum, trimethylgallium, and ammonia (NH_3) were used as precursors of Al, Ga, and N, respectively. Hydrogen (H_2) and nitrogen (N_2) were used as the carrier gases. Initially, a 20 nm thick low-temperature (LT) AlN nucleation layer (NL) was deposited on the sapphire substrate at 850°C. A 2.8 μm high-temperature (HT) AlN template was subsequently grown under 1250°C, followed by 50 pairs of AlN/AlGaN superlattices used as dislocation filters. Then, a 2 μm Si-doped n-$Al_{0.6}Ga_{0.4}$ contact layer was deposited. Afterwards, four pairs of $Al_{0.4}Ga_{0.6}N/Al_{0.55}Ga_{0.45}N$ MQWs were grown under 1050°C. A 20 nm p-$Al_{0.7}Ga_{0.4}N$ electron barrier layer (EBL), 50 nm p-$Al_{0.65}Ga_{0.45}N$ layer, and 50 nm p^+-GaN contact layer were subsequently deposited. Surface morphologies and spatially resolved current distributions of the UV LEDs were characterized by a Veeco Dimension 3100V conductive atomic force microscope (CAFM) in contact mode with a Pt-coated Si probe. Crystalline qualities were analyzed using a point-focused high-resolution X-ray (Cu Ka1) diffractometer (HRXRD, Bruker D8 DISCOVER) equipped with a four-bounce symmetric Ge (220) monochromator. PL studies were performed using a Coherent Ar-F (193 nm) excimer laser at pumping power of 50 $mW \cdot cm^{-2}$, collected by a Horiba iHR550 spectrometer. Electroluminescence (EL) was analyzed by a Keithley 4200-SCS semiconductor characterization system. Electron channeling contrast imaging (ECCI) investigation was performed using a Verios G4 UC characterization system with voltage of 20 kV. Transmission electron microscopy (TEM) samples were prepared using an FEI^{TM} Helios dual-beam focused ion beam scanning electron microscope system with a Ga ion source. Thicknesses of MQWs and dislocation distributions were characterized by an FEI probe-corrected Titan high-angle annular dark-field imaging-scanning transmission electron microscopy (HAADF-STEM) system operated at an acceleration voltage of 300 kV. All measurements were performed at room temperature (RT).

3. RESULTS AND DISCUSSION

As reported by numerous researchers, the misoriented angle of sapphire substrate strongly influences the growth kinetics of AlN and AlGaN thin films, and correspondingly, leads to dramatically different optoelectronic performances [20–23]. MQWs or UV LEDs grown on highly misoriented sapphire exhibit step-bunching surface morphology. To investigate the correlation between surface morphology and current distribution under forward and reverse biases, CAFM was carried out. After a series of surface cleaning steps, a UV LED wafer was loaded into a tightly sealed glove box where the CAFM characterization was performed under the flow of dry N_2 gas. The purpose is to minimize surface oxidation during characterization. The current distributions were probed in contact mode on top of the p-GaN layer, and the sample bias voltage was applied to the substrate with respect to the tip. The schematic image of the setup as well as the sample structure is shown in the inset of Fig. 1(a). During scanning, the probe was in contact with the sample surface under constant repulsive force in the range of 10–40 nN. The range of detectable currents is 10 to 500 nA for the CAFM module amplifier.

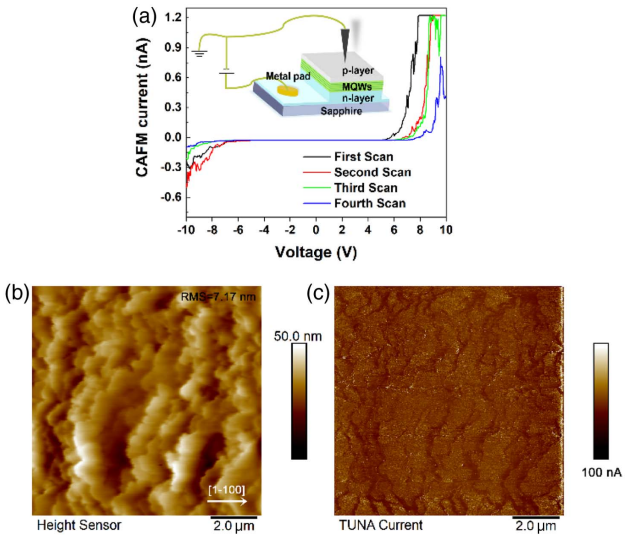

Fig. 1. (a) Schematic setup of CAFM and four consecutive I–V curves during the scans; (b) typical surface morphology of UV LED grown on a 1° misoriented sapphire substrate; and (c) corresponding current distribution map under forward bias of +7 V.

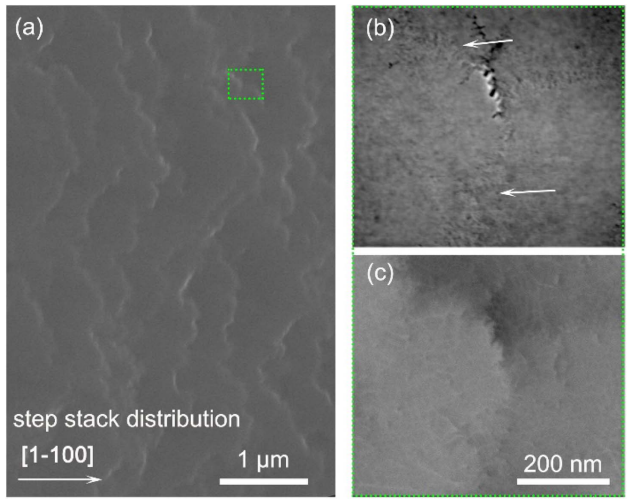

Fig. 2. (a) Top view SEM image of the surface of UV LED; (b) zoom-in view image near the step edge as indicated by the green box and (c) corresponding ECCI graph.

The current-voltage (I-V) curves shown in Fig. 1(a) represent a local electrical behavior near the step edge within the voltage range of −10 to +10 V. The I-V characterization was performed consecutively 4 times. When forward voltage bias (0–10 V) was applied to the surface, even though the turn-on voltage increases with the scan proceeding, the local current becomes saturated at higher bias, indicating a stable current pathway. However, when UV LED is under reverse bias (−10 to 0 V), the reverse current reduces as the number of scans increases and finally becomes negligible. Prior CAFM studies show that dislocations may serve as channels for large and stable reverse-bias leakage current [24]. This is in contrast with the observation in this work, suggesting that the local current distributions in the UV LEDs are not associated with dislocations. From the surface morphology image shown in Fig. 1(b), large numbers of step bunching are formed on the surface. Spradlin *et al.* found a significant decrease in reverse bias current after several scans and attributed this phenomenon to "charge trapping effects" [25]. It is believed that the same phenomenon occurred in this work. When the reverse bias is applied to the surface, electrons tend to fill the potential minima. When the potential minima are saturated, the reverse-bias current becomes negligible. Figure 1(c) illustrates the current distribution under forward bias of +7 V, in which case the LED is already turned on. Higher current is represented by the dark contrast in the map, which corresponds perfectly with the step edges, indicating that under forward bias, the current is mainly localized on the step edges due to carrier localization effect, and a strong dependence on the surface morphology is therefore obtained.

Scanning electron microscope (SEM) images with low magnification across several step edges of the UV LED were taken; the results are shown in Fig. 2(a). Step edges can be clearly observed extending from the top to the bottom of the image facing toward the [1−100] direction, which are consistent with the results from AFM morphology. In the meantime, these step edges are obviously different from the rough surface induced by Mg doping or dislocation-associated spirals, where the orientations are randomly distributed [26,27]. Figures 2(b) and 2(c) show high-resolution SEM and ECCI images. The step edges are marked by white arrows in Fig. 2(b). The applied acceleration voltage of the ECCI system is 20 kV; thus the dislocation information within approximately 700 nm below the surface is obtained [23]. From Fig. 2(c), dislocations illustrated by the slight contrast difference distribute randomly on the surface, and no obvious correlation between the dislocations and step edges is revealed. The TDD is estimated to be $\sim 6 \times 10^9$ cm^{-2} from ECCI image. HRXRD rocking curves (RCs) of the (002) and (102) reflections of n-type AlGaN layer below the MQW were also performed, providing a TDD of 8.6×10^9 cm^{-2}, which is slightly higher than that calculated from ECCI. Considering that the sample contains multiple epitaxial layers with different compositions, the contrast difference of the dislocations shown in ECCI might be reduced, leading to underestimation of the TDD. Nevertheless, despite the marginal difference, the step bunching features on the sample surface are clearly not correlated with underlying dislocations. This observation has the important implication that step bunches on the surface will not act as current leakage paths during device turn-on, and thus will not adversely affect the electrostatic discharge (ESD) properties of UV LEDs. On the contrary, the formation of step bunches will suppress the propagation of edge-type dislocations, as we previously reported [15], which is believed to be beneficial for stable UV emission.

Cross-sectional HAADF-STEM was performed near the MQW region of the sample to illustrate the microscale features. Figures 3(a) and 3(b) show the two-beam dark-field images taken with vector of $g = [0002]$ and $g = [1120]$. Screw-type and mixed-type threading dislocations (TDs) are noticeable with $g = [0002]$, while edge-type and mixed-type TDs are noticeable with $g = [1120]$ [28]. From Figs. 3(a) and 3(b), we can

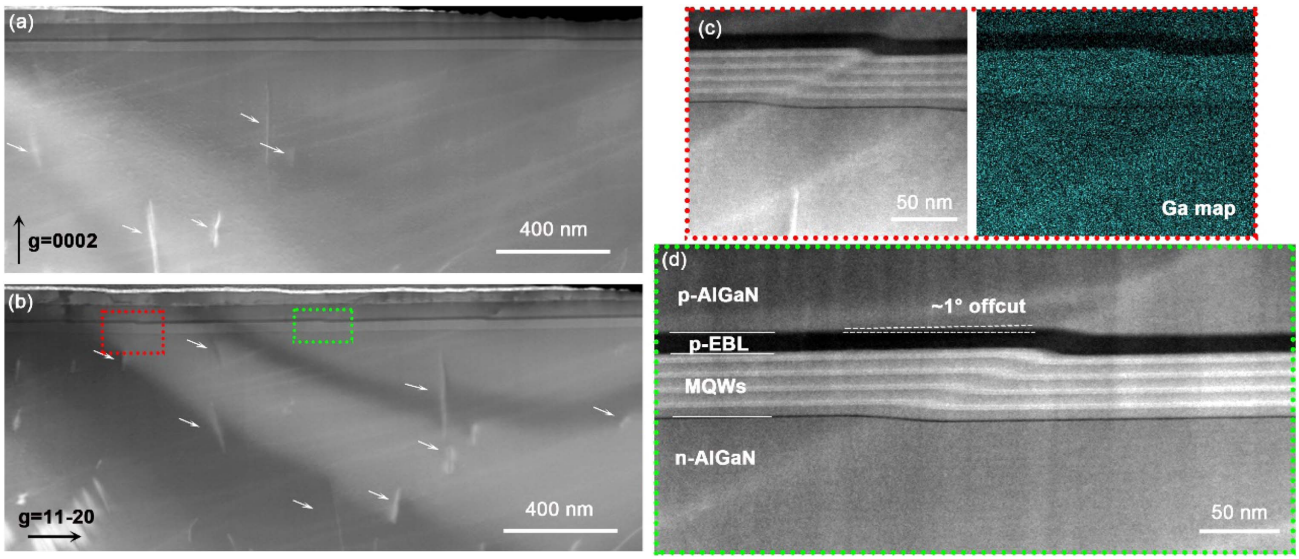

Fig. 3. (a) Cross-sectional $g = [0002]$ and (b) $g = [11–20]$ dark-field TEM images under two-beam conditions for UV LED grown on a 1° misoriented sapphire substrate; (c) cross-sectional image of the MQW and corresponding Ga EDS mapping near the step edge; (d) zoom-in view of the MQW regions.

ascertain that these two kinds of dislocations distribute randomly in the n-AlGaN template, as indicated by the white arrows, and most of the dislocations annihilate below the MQWs. This further proves that the current paths in the CAFM image are not associated with threading dislocations. Large kinks or step edges are uniformly distributed along the MQWs with a lateral distance of ~500 nm. These step edges on the epitaxial thin films are directly caused by a 1° misorientation angle of the sapphire substrate, which has been previously discussed by other researchers [18]. Below the step edges, white streaks are revealed with a tilt angle of approximately 30° toward the (0001) plane. Most of these streaks are associated with the IQWs. In Fig. 3(c), an EDS mapping of the Ga element is illustrated, and the white streaks are Ga-rich, clearly suggesting that composition inhomogeneity occurs from the beginning of AlGaN thin film, consistent with other reports [18,29]. The Ga-rich streaks are most likely due to the mass transport of Ga adatoms from terrace surfaces to the kinks or edges of macro-steps during crystal growth, since a Ga adatom has a much longer diffusion length than Al [21].

Figure 3(d) shows the zoom-in view of the MQWs near the step edge. The orientation and thickness of Ga-deficient and Ga-rich layers of the sample can be distinguished by the dark and bright contrast, respectively [30]. The MQW is 1° tilted relative to the (0001) crystallographic plane, as indicated by the white dashed line in Fig. 3(d), in accordance with the substrate misorientation angle of ~1°. Thickness expansion or even twist of the QWs can be observed at the edge. The width of the AlGaN QWs grown on the flat surface is ~3 nm, while the width slightly expands to ~3.5 nm near the step edges. Even though the exact composition difference in the step edges is not known, there is no denying that thickness and composition fluctuation will result in lower bandgap. This would in turn lead to the different electrical and optical behaviors of the UV LEDs.

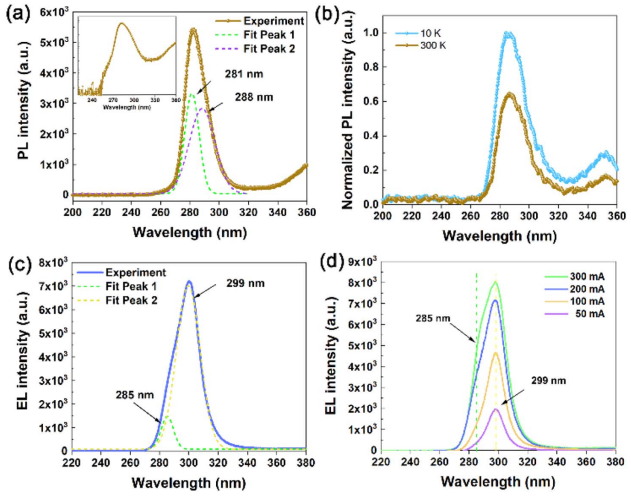

Fig. 4. (a) RT PL spectrum of UV LED grown on a 1° misoriented sapphire substrate; (b) PL spectra of UV LED under RT and LT; (c) RT EL spectrum of the same sample under current injection of 200 mA; (d) EL spectra under injection currents ranging from 50 to 300 mA.

RT PL and EL were further studied to verify the relationship between composition/thickness fluctuation and luminescence properties of the UV LEDs. In the PL spectrum shown in Fig. 4(a), an obvious sub-300 nm MQW emission is revealed. The PL spectrum can be deconvoluted into two distinct peaks at wavelengths 281 and 288 nm, respectively. Besides, a weak 255 nm side emission peak is expected to come from n-$Al_{0.6}Ga_{0.4}N$ with a bandgap of 4.77 eV. Note that the wavelength at 281 nm is the targeted emission of the MQWs. Therefore, the longer 288 nm emission may originate from the step-edge area with higher Ga composition and thicker

QW. It is found that 281 nm peak is stronger than the 288 nm peak from the PL spectrum. It is worth noting that the maximum carrier diffusion length in AlGaN is about 40–70 nm [22], much smaller than the average terrace width of ~500 nm. Therefore, not all the photogenerated carriers can diffuse into the IQWs and contribute to the 288 nm emission, even though the IQW has a relatively lower surface potential. Thus, the larger proportion of the 281 nm emission peak from Fig. 4(a) may simply originate from the relatively larger area of the flat MQWs as revealed by TEM. The IQE value of the UV LED was also obtained by taking the ratio of the integrated intensity of the PL spectra from RT (300 K) to that in LT, under the assumption that nonradiative recombination centers are frozen under LT (10 K). As shown in Fig. 4(b), IQE reaches ~63%, which is among the highest values of UVB LEDs [12,20], suggesting the high radiative recombination rate in the active regions due to composition localization of Ga and Al.

Figure 4(c) illustrates the EL spectrum of the UV LED under an injection current of 200 mA. There are also two emission peaks located at wavelengths of 287 and 298 nm. Due to strong UV absorption in the p-GaN contact layer, PL characterization was performed under high pumping power, leading to a strong band filling effect and thus blueshift of the peak position. More importantly, during optical pumping, both Ga-rich and Ga-deficient regions are uniformly excited. On the contrary, under electrical injection condition, photons mostly come from Ga-rich regions in UV LEDs due to the carrier localization effect. As a consequence, PL exhibits a shorter emission wavelength compared to EL. In addition, note that the intensity of the longer-wavelength emission peak is stronger than that of the shorter-wavelength one in Fig. 4(c). This is in contrast with the PL spectrum, suggesting that under current injection, carriers are more inclined to pass through the IQW region, where the carrier localization effect is enhanced. Note that from the CAFM result in Fig. 1, current is mainly localized in the step edges when the device is turned on, confirming that EL characterization is highly dependent on the surface morphology. To demonstrate this hypothesis, EL spectra under various injection currents from 50 to 300 mA are shown in Fig. 4(d). A shorter-wavelength peak can barely be seen under the low injection current, while as the current injection increases, the intensity of the shorter-wavelength emission peak increases significantly. This can be ascribed to the saturation of the current paths at the step edges, which will be further discussed later on.

Furthermore, light output power and the corresponding EQE value of the UV LED grown on 1° misoriented sapphire substrate were characterized on a 2-inch (1 inch = 2.54 cm) bare wafer using an integrating sphere, with operation condition in CW mode. *I-V* curve and EL spectra under the currents of 5–80 mA are shown in Figs. 5(a) and 5(b), and the EQE value as a function of injection current is shown in Fig. 5(c). The turn-on voltage is about 7 V, and there is no obvious current leakage when a reverse bias of −5 V is applied on the UV LED, as shown in the inset of Fig. 5(a). The output power increases almost linearly with the applied current, while the EQE value increases rapidly at first and then slowly decreases. The peak EQE value is estimated to be 1.23% at the current level of 40 mA. Due to the configuration of our test method, EQE value is expected to be even higher after packaging of the UV LED chip.

Although the step bunch has offered a unique advantage of carrier localization, the detailed mechanism on the contribution of step bunching to the performance of the UV LEDs is still unclear [16]. Herein, a simple UV LED structure containing both inclined and flat QWs was proposed and the EL property was numerically simulated. A single QW was adopted in this model to reduce computational load and avoid convergence problems. Self-consistent solutions to the basic semiconductor equations, including Poisson, continuity, and drift-diffusion transport equations, were obtained using finite-element analysis. The appropriate boundary conditions, in addition to Shockley–Read–Hall (SRH), radiative, Auger, and surface recombination were all considered in this model. In order to guarantee the results obtained from simulation are universal, all of the physical parameters used in this model are the same as a flat *c*-plane UV LED, and the parameters such as composition and thickness are completely borrowed from the STEM results shown in Fig. 3. The modeled detailed structure and composition distribution are shown in Fig. 6(a). An IQW is located in the middle of the active region. Similar to that observed from STEM, a Ga-rich stripe penetrates all the AlGaN layers, and the composition fluctuation follows Gaussian distribution. This model is simulated under the applied bias of +6 V, and the radiative recombination rate and the total current distribution are shown in Figs. 6(b) and 6(c), respectively.

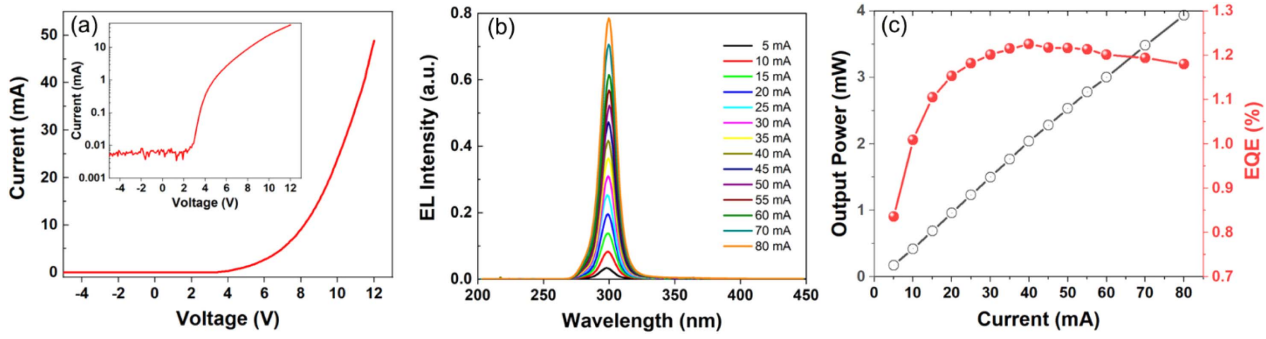

Fig. 5. (a) *I-V* curve; (b) EL spectra under different injection currents from 5 to 80 mA; (c) light output power and estimated EQE as functions of injection current.

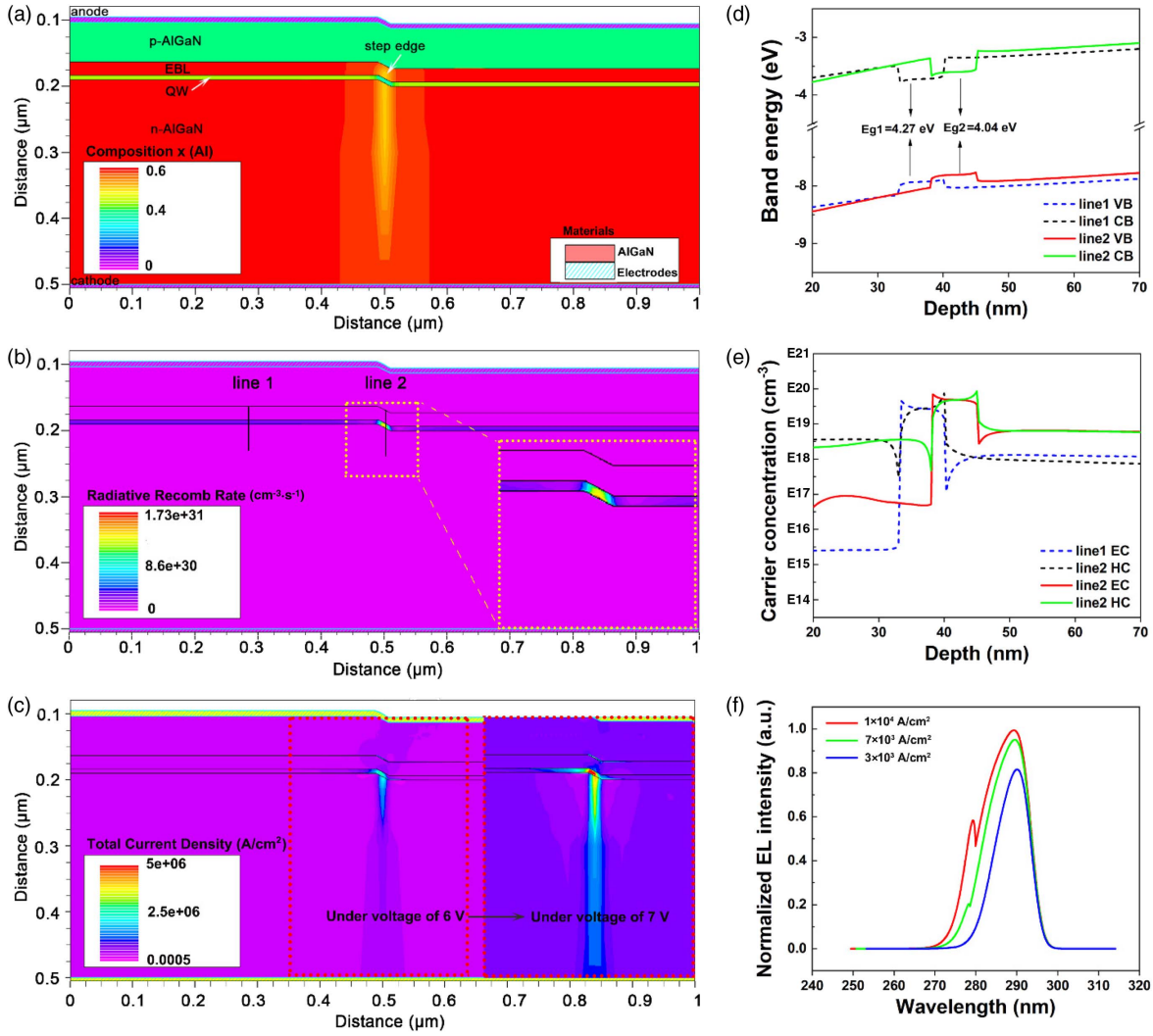

Fig. 6. (a) Schematic structure and composition distribution of a UV LED with single QW in the simulation; (b) the distribution of radiative recombination rate; and (c) total current distribution; (d) the energy band structure and (e) distribution of carrier concentration of the flat and inclined active region, respectively. EC and HC stand for electron concentration and hole concentration. (f) EL spectra of the UV LED under different current densities.

Due to the potential minimum in the IQW region, the radiative recombination behavior is well confined in the QW, and a maximum of radiative recombination rate is obtained in the step edge, as illustrated in Fig. 6(b). The current distribution mapping shown in Fig. 6(c) indicates that under forward bias, carriers are mainly concentrated on the step edges. This phenomenon is in perfect agreement with the CAFM results. Data along two vertical lines across the active region of flat and inclined QW were extracted from Fig. 6(b), and the results are plotted in Figs. 6(d) and 6(e), respectively. Both QWs show strong band bending caused by the spontaneous polarization and external electric field. The IQW has a smaller bandgap ($E_{g2} = 4.04$ eV) compared to the flat QW ($E_{g1} = 4.27$ eV) due to higher Ga component. Higher carrier concentration is observed in the IQW, and better overlap of the wave functions of electrons and holes is expected. Note that MQWs grown on nonpolar or semipolar surfaces have weaker quantum-confined stark effect, leading to higher IQE value [31]. Nevertheless, nonpolar and semipolar MQWs usually suffer from low crystalline quality and rough surface morphology, detracting from their advantages. In comparison, the unique orientation of the IQW was unambiguously verified as having the same advantage as nonpolar and semipolar MQWs, but at the same time, with much lower threading dislocations. The carriers are mainly confined in the IQW, forming an effective radiative recombination center. Therefore, the selective injection of current and stronger carrier localization should be considered as the two major factors contributing to the higher IQE and superior performance of UV LED grown on a misoriented substrate.

Figure 6(f) shows the simulated EL spectra under the injection current densities of 3×10^3, 7×10^3, and 1×10^4 A/cm^2. Single peak emission at 290 nm is observed under 3×10^3 A/cm^2, while double peaks appear when the current increases. Note that the current is mainly concentrated in the step edge when a relatively low current density of 3×10^3 A/cm^2 at the bias of +6 V is applied on the sample [Fig. 6(c)]. When the current density increases to 1×10^4 A/cm^2, current

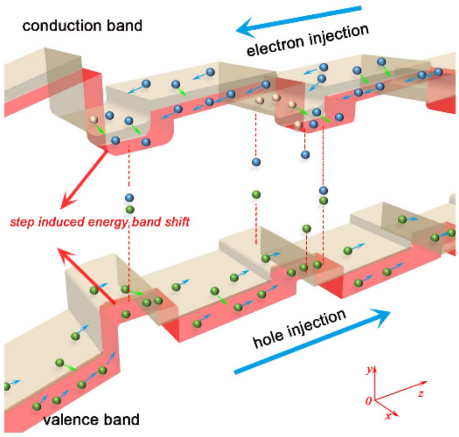

Fig. 7. Proposed 3D schematic band diagram of the active region of the UV LED across the step-bunched region.

spreads to the periphery of the step edge region, as shown in the inset in Fig. 6(c). This is clearly demonstrated by the occurrence of a high-energy side peak from the simulation result. Therefore, under the condition of high current density injection, carrier delocalization occurs, and the current distribution becomes more uniform.

As mentioned above, Ga-rich stripes accompany the step edges, leading to strong band bending and carrier localization effect. A schematic three-dimensional (3D) energy band structure of the active region containing the IQW was therefore proposed according to the experimental and simulation results. As shown in Fig. 7, EBL, QW, and quantum barrier (QB) are shown from left to right. The fluctuation of the bandgap along the x axis is illustrated by the red region. This "3D band diagram" is induced by the Ga localization effect at the step edges. The blue arrows indicate the direction of electron and hole injections, while the green arrows represent the process of carrier localization, deviating away from majority of the carriers that transport along the c axis. Due to their higher carrier concentration and higher radiative recombination rate, the IQWs have higher IQE value, thus boosting the output power of the UV LED. The schematic diagram illustrates that the underlying mechanism of UV LEDs grown on misoriented sapphire is due to the unique band structure and carrier transportation process. This study also proves that in the AlGaN ternary compound, it is feasible to adopt quantum wires or quantum dots to improve the luminous efficiency of UV LEDs without sacrificing their crystalline quality.

Interestingly, step-bunching-induced Ga phase separation not only appears in AlGaN grown on high misorientation sapphire. Similar phenomena have been observed in MQWs grown on low misorientation substrate or even on-axis sapphires, where nitride thin films exhibit step-flow growth morphology [6,17,32]. Carrier localization has always been a common observation in III-nitrides, especially InGaN. Currents prefer to reside in the potential minima. The investigations shown in this work are in fact valid for all ternary III-V semiconductor systems exhibiting phase separation, including III-arsenide. Understanding the carrier transport and recombination behaviors in such thin films can greatly help us to improve the performance of III-V semiconductor devices.

4. CONCLUSION

In summary, a sub-300 nm UVB LED with IQE of 63% and EQE of 1.23% was designed and fabricated on a 1° misoriented sapphire substrate. Direct evidence on carrier transportation and recombination on step-bunched surface of UV-LED was provided. The current distribution strongly follows the surface morphology of the thin film. Top view ECCI and cross-sectional HAADF-STEM demonstrated that these current paths are not associated with threading dislocations, but rather are related to the step edges with Ga-rich potential minima. This structure was further modeled and simulated by solving the Poisson equations and carrier transport equations. An efficient recombination center is formed in the IQWs owing to higher carrier concentration and larger radiative recombination rates. Finally, a schematic diagram of a 3D energy band structure of the active region of the UV LED across the step edges was proposed.

Funding. National Key Research and Development Program of China (2016YFB0400802); National Natural Science Foundation of China (61974149); Key Research and Development Program of Zhejiang Province (2019C01080, 2020C01145); Science and Technology Innovation 2025 Major Project of Ningbo (2018B10088, 2019B10121); Instrument Developing Project of the Chinese Academy of Sciences (YJKYYQ20190074).

Acknowledgment. The authors appreciate the technical support from Nano Fabrication Facility, Platform for Characterization & Test in Ningbo Institute of Materials Technology and Engineering, CAS.

Disclosures. The authors declare no conflicts of interest.

REFERENCES

1. C. Zhou, A. Ghods, V. G. Saravade, P. V. Patel, K. L. Yunghans, C. Ferguson, Y. Feng, B. Kucukgok, N. Lu, and I. T. Ferguson, "Review—the current and emerging applications of the III-nitrides," ECS J. Solid State Sci. Technol. **6**, Q149–Q156 (2017).
2. M. Kneissl and J. Rass, *III-Nitride Ultraviolet Emitters: Technology and Applications* (Springer, 2016).
3. S. Matsuura and S. Ishikura, "Suppression of tomato mosaic virus disease in tomato plants by deep ultraviolet irradiation using light-emitting diodes," Lett. Appl. Microbiol. **59**, 457–463 (2014).
4. P. J. Hargis, T. J. Sobering, G. C. Tisone, J. Wagner, S. A. Young, and R. J. Radloff, "Ultraviolet fluorescence identification of protein, DNA, and bacteria," Proc. SPIE **2366**, 147–153 (1995).
5. K. Song, M. Mohseni, and F. Taghipour, "Application of ultraviolet light-emitting diodes (UV-LEDs) for water disinfection: a review," Water Res. **94**, 341–349 (2016).
6. M. X. Wang, F. J. Xu, N. Xie, Y. H. Sun, B. Y. Liu, Z. X. Qin, X. Q. Wang, and B. Shen, "Crystal quality evolution of AlN films via high temperature annealing under ambient N_2 conditions," CrystEngComm **20**, 6613–6617 (2018).
7. S. Zlotnik, J. Sitek, K. Rosiński, P. P. Michałowski, J. Gaca, M. Wójcik, and M. Rudziński, "Growth and thermal annealing for acceptor activation of p-type (Al)GaN epitaxial structures: technological challenges and risks," Appl. Surf. Sci. **488**, 688–695 (2019).
8. H. Xu, H. Long, J. Jiang, M. Sheikhi, L. Li, W. Guo, J. Dai, C. Chen, and J. Ye, "Strain modulated nanostructure patterned AlGaN-based

deep ultraviolet multiple-quantum-wells for polarization control and light extraction efficiency enhancement," Nanotechnology **30**, 435202 (2019).
9. N. Maeda and H. Hirayama, "Realization of high-efficiency deep-UV LEDs using transparent p-AlGaN contact layer," Phys. Status Solidi C **10**, 1521–1524 (2013).
10. N. Susilo, S. Hagedorn, D. Jaeger, H. Miyake, U. Zeimer, C. Reich, B. Neuschulz, L. Sulmoni, M. Guttmann, F. Mehnke, C. Kuhn, T. Wernicke, M. Weyers, and M. Kneissl, "AlGaN-based deep UV LEDs grown on sputtered and high temperature annealed AlN/sapphire," Appl. Phys. Lett. **112**, 041110 (2018).
11. M. A. Khan, N. Maeda, M. Jo, Y. Akamatsu, R. Tanabe, Y. Yamada, and H. Hirayama, "13 mW operation of a 295–310 nm AlGaN UV-B LED with a p-AlGaN transparent contact layer for real world applications," J. Mater. Chem. **7**, 143–152 (2019).
12. M. Kneissl, T. Y. Seong, J. Han, and H. Amano, "The emergence and prospects of deep-ultraviolet light-emitting diode technologies," Nat. Photonics **13**, 233–244 (2019).
13. P. Dong, J. Yan, J. Wang, Y. Zhang, C. Geng, T. Wei, P. Cong, Y. Zhang, J. Zeng, Y. Tian, L. Sun, Q. Yan, J. Li, S. Fan, and Z. Qin, "282-nm AlGaN-based deep ultraviolet light-emitting diodes with improved performance on nano-patterned sapphire substrates," Appl. Phys. Lett. **102**, 241113 (2013).
14. K. Ban, J. Yamamoto, K. Takeda, K. Ide, M. Iwaya, T. Takeuchi, S. Kamiyama, I. Akasaki, and H. Amano, "Internal quantum efficiency of whole-composition-range AlGaN multiquantum wells," Appl. Phys. Express **4**, 052101 (2011).
15. H. Xu, J. A. Jiang, M. Sheikhi, Z. Chen, J. Hoo, S. Guo, W. Guo, H. Sun, and J. Ye, "Single peak deep ultraviolet emission and high internal quantum efficiency in AlGaN quantum wells grown on large miscut sapphire substrates," Superlattices Microstruct. **129**, 20–27 (2019).
16. H. Sun, S. Mitra, R. C. Subedi, Y. Zhang, W. Guo, J. Ye, M. K. Shakfa, T. K. Ng, B. S. Ooi, I. S. Roqan, Z. Zhang, J. Dai, C. Chen, and S. Long, "Unambiguously enhanced ultraviolet luminescence of AlGaN wavy quantum well structures grown on large misoriented sapphire substrate," Adv. Funct. Mater. **29**, 1905445 (2019).
17. M. Hou, Z. Qin, L. Zhang, T. Han, M. Wang, F. Xu, X. Wang, T. Yu, Z. Fang, and B. J. S. Shen, "Excitonic localization at macrostep edges in AlGaN/AlGaN multiple quantum wells," Superlattices Microstruct. **104**, 397–401 (2017).
18. H. Kojima, T. Ogasawara, M. Kim, Y. Saito, K. Iida, N. Koide, T. Takeuchi, M. Iwaya, S. Kamiyama, and I. Akasaki, "Sapphire substrate off-angle and off-direction dependences on characteristics of AlGaN-based deep ultraviolet light-emitting diodes," Jpn. J. Appl. Phys. **58**, sc1025 (2019).
19. T. Kolbe, A. Knauer, J. Enslin, S. Hagedorn, A. Mogilatenko, T. Wernicke, M. Kneissl, and M. Weyers, "Influence of substrate off-cut angle on the performance of 310 nm light emitting diodes," J. Cryst. Growth **526**, 125241 (2019).
20. Y. H. Sun, F. J. Xu, N. Xie, J. M. Wang, N. Zhang, J. Lang, B. Y. Liu, X. Z. Fang, L. B. Wang, W. K. Ge, X. N. Kang, Z. X. Qin, X. L. Yang, X. Q. Wang, and B. Shen, "Controlled bunching approach for achieving high efficiency active region in AlGaN-based deep ultraviolet light-emitting devices with dual-band emission," Appl. Phys. Lett. **116**, 212102 (2020).
21. Y. Nagasawa, R. Sugie, K. Kojima, A. Hirano, M. Ippommatsu, Y. Honda, H. Amano, I. Akasaki, and S. F. Chichibu, "Two-dimensional analysis of the nonuniform quantum yields of multiple quantum wells for AlGaN-based deep-ultraviolet LEDs grown on AlN templates with dense macrosteps using cathodoluminescence spectroscopy," J. Appl. Phys. **126**, 215703 (2019).
22. M. Hayakawa, S. Ichikawa, M. Funato, and Y. Kawakami, "$Al_xGa_{1-x}N$-based quantum wells fabricated on macrosteps effectively suppressing nonradiative recombination," Adv. Opt. Mater. **7**, 1801106 (2019).
23. K. Jiang, X. Sun, J. Ben, Z. Shi, Y. Jia, Y. Wu, C. Kai, Y. Wang, and D. Li, "Suppressing the compositional nonuniformity of AlGaN grown on HVPE-AlN template with large macro-steps," CrystEngComm **21**, 4864–4873 (2019).
24. D. Liu, S. J. Cho, H. Zhang, C. Carlos, R. Kalapala, J. Park, J. Kim, R. Dalmau, J. Gong, B. Moody, X. Dong, J. D. Albrecht, W. Zhou, and Z. Ma, "Influences of screw dislocations on electroluminescence of AlGaN/AlN-based UVC LEDs," AIP Adv. **9**, 085128 (2019).
25. J. Spradlin, S. Dogan, J. Xie, R. J. Molnar, A. A. Baski, and H. Morkoc, "Investigation of forward and reverse current conduction in GaN films by conductive atomic force microscopy," Appl. Phys. Lett. **84**, 4150–4152 (2004).
26. S. Walde, S. Hagedorn, P.-M. Coulon, A. Mogilatenko, C. Netzel, J. Weinrich, N. Susilo, E. Ziffer, L. Matiwe, C. Hartmann, G. Kusch, A. Alasmari, G. Naresh-Kumar, C. Trager-Cowan, T. Wernicke, T. Straubinger, M. Bickermann, R. W. Martin, P. A. Shields, M. Kneissl, and M. Weyers, "AlN overgrowth of nano-pillar-patterned sapphire with different offcut angle by metalorganic vapor phase epitaxy," J. Cryst. Growth **531**, 125343 (2020).
27. N. Susilo, J. Enslin, L. Sulmoni, M. Guttmann, U. Zeimer, T. Wernicke, M. Weyers, and M. Kneissl, "Effect of the GaN:Mg contact layer on the light-output and current-voltage characteristic of UVB LEDs," Phys. Status Solidi A **215**, 1700643 (2018).
28. F. Ponce, D. Cherns, W. T. Young, and J. W. Steeds, "Characterization of dislocations in GaN by transmission electron diffraction and microscopy techniques," Appl. Phys. Lett. **69**, 770–772 (1996).
29. K. Kojima, Y. Nagasawa, A. Hirano, M. Ippommatsu, Y. Honda, H. Amano, I. Akasaki, and S. F. Chichibu, "Carrier localization structure combined with current micropaths in AlGaN quantum wells grown on an AlN template with macrosteps," Appl. Phys. Lett. **114**, 011102 (2019).
30. W. Guo, H. Sun, B. Torre, J. Q. Li, M. Sheiki, J. Jiang, H. Li, S. Guo, K. Li, R. Lin, A. Giugni, E. D. Fabrizio, X. Li, and J. Ye, "Lateral polarity structure of AlGaN quantum wells: a promising approach to enhancing the ultraviolet luminescence," Adv. Funct. Mater. **28**, 1802395 (2018).
31. H. Masui and S. Nakamura, "Nonpolar and semipolar orientations: material growth and properties," Mater. Sci. Forum **590**, 211–232 (2008).
32. J. Yan, J. Wang, Y. Zhang, P. Cong, L. Sun, Y. Tian, C. Zhao, and J. Li, "AlGaN-based deep-ultraviolet light-emitting diodes grown on high-quality AlN template using MOVPE," J. Cryst. Growth **414**, 254–257 (2015).